INVESTIGATION OF POWER CONVERSION EFFICIENCY OF A DYE-SENSITIZED SOLAR CELL FABRICATED USING GREEN-SYNTHESIZED ZINC OXIDE NANOPARTICLES AS PHOTO-ANODE

BALABYE STEPHEN

21/U/GMSP/14078/PE

A DISSERTATION SUBMITTED TO THE DIRECTORATE OF RESEARCH AND GRADUATE TRAINING IN PARTIAL FULFILMENT AS A REQUIREMENT FOR THE AWARD OF THE DEGREE OF MASTER OF SCIENCE IN PHYSICS OF KYAMBOGO UNIVERSITY

SEPTEMBER 2025

DECLARATION

I, Balabye Stephen, hereby declare that this work titled "Investigation of Power Conversion Efficiency of a Dye-sensitized Solar cell fabricated using Green-Synthesized Zinc Oxide Nanoparticles as Photo-anode" has never been presented to any Higher Education Institution for consideration of any similar award.

Signature ……. Date ……..……

APPROVAL

This is to certify that this research dissertation by Balabye Stephen titled "Investigation of Power Conversion Efficiency of a Dye-sensitized Solar cell fabricated using Green Synthesized Zinc Oxide Nanoparticles as Photo- anode" has been done under our supervision and is now duly approved for submission to the Directorate of Research and Graduate Training, and Senate of Kyambogo University.

Signature ……Date …….

Dr. Mukhokosi Emma Panzi

Principal supervisor

Department of Physics, Kyambogo University

Signature…….... Date……

Dr. Egor Moses

Co-supervisor

Department of Chemistry, Busitema University

DEDICATION

This scholarly writing is dedicated to my wife Kagoya Ruth for her continued support and prayers she exhibited to me in this academic journey specifically at this level. May the good Lord greatly bless her.

ACKNOWLEDGEMENT

I thank God the Almighty, for the gift of life and protection throughout the preparation of this dissertation.

I am greatly thankful to all my lecturers in the Physics Department of Kyambogo University for the guidance they gave to me, the laboratory technicians of Physics and Biology departments; Mr. Kawuki Joseph, Mr. Balimunsahe John and Mr. Isabirye Isaac for their technical advice and guidance in the process of sample preparations.

I owe much debt to my principal supervisor, Dr. Mukhokosi Emma Panzi and the co-supervisor, Dr. Egor Moses for their educative advice, continuous guidance and encouragement which led to the successful completion of this dissertation.

I thank my course mates Nzuguwa Michael Evans, Stephen Tenywa, Tibenkana Mohammed, Ssikubwabo Ivan and Muhindo Nyansiyo for the cooperation and great assistance during the course of study.

I further extend my gratitude to my mother Nabirye Jane, all relatives and friends for their moral and spiritual support. May the Almighty God bless the work of your hands and reward you abundantly.

TABLE OF CONTENTS

LIST OF FIGURES

LIST OF TABLES

ABSTRACT

Green synthesis, a biological method for nanoparticle preparation, has been suggested as a possible eco-friendly alternative to chemical and physical methods. In this study, green synthesis of zinc oxide (ZnO) nanoparticles (NPs) from *Erythrina abyssinica* stem bark extract calcined under different temperatures (300-700 ℃) for application as a photo-anode in dye sensitized solar cells (DSSCs) was carried out. Synthesized ZnO Nps were subjected to characterization using X-Ray diffraction (XRD), Scanning Electron Microscope (SEM), Energy Dispersive X-ray Spectroscopy (EDX), Visible (UV-Vis) Spectroscopy and photo luminescence (PL) analysis. The analysis revealed that highly crystalline hexagonal ZnO NPs were formed at 700 ℃, with the nanospheres agglomeration into non-uniform distinct NPs with a band gap energy of 3.12 eV. An efficient dye sensitized solar cell (DSSC) was fabricated with synthesized ZnO Nps as photo- anode materials. The fabricated DSSC showed an open circuit voltage (V_{oc}) of 161 mV, short circuit current density(J_{sc}) of 56 μAcm^{-2}, a Fill factor of 0.265 and a power conversion efficiency (PCE) of 2.4×10^{-2} % under one sun illumination. The low value of efficiency can be attributed to the limited light absorption in the visible spectrum by the ruthenium N719 dye adsorbed on the biosynthesized ZnO nanoparticles, and fast electron-hole recombination rate. Further research should be focused on improving the light absorption range of Ru N719 dye adsorbed on biosynthesized ZnO nanoparticles and minimizing the charge recombination rates through doping and heterostructuring.

Keywords: ZnO, Green synthesis, DSSCs

CHAPTER ONE: INTRODUCTION

1.1 Background of the Study

The life style that is centered on power consuming devices and machinery is a notable aspect of modern society. Currently the estimated energy consumption for the global population of seven billion is about 13 terawatts (TW) and this figure is projected to increase by an additional 10 TW by the year 2050 (McNeill & Engelke, 2022). Resources for fossil fuels are few and rapidly running out. As a result renewable energy sources are currently on a high demand (Chandra et al., 2019) to power the activities of today's society. Hydroelectric energy, wind energy, geothermal energy and solar energy are some of the sources which are renewable. Despite geographical limitations of the first three energy sources, solar energy is the most abundant source of energy on earth (Chandra et al., 2019). Solar energy can be tapped by photovoltaic (PV) technology. Three generations of solar cells have been developed as a result of thorough research into PV technology (Kishore Kumar et al., 2020) ; the first, second, and third generations. However, the production of first and second-generation solar cells is expensive, making them un affordable for the poor communities.

The most significant alternative for transforming sun light energy into electric power is the third-generation solar cell called a dye-sensitized solar (DSSC) due its simple production method, low manufacturing costs, and environmental friendliness (Fadhlan et al., 2020). The nanoparticles from semiconductor oxides such as titanium dioxide (TiO_2) and zinc oxide (ZnO) can be used to make its photo-anode. Recent scientific progress in DSSCs have concentrated on enhancing electron transport and minimizing the recombination rate by utilizing

semiconductor materials other than TiO_2 (Tata et al., 2020). Among the feasible alternatives is Zinc oxide (ZnO), an n-type semiconductor with a wide bandgap of about 3.37 eV and is nontoxic. ZnO can be processed chemically or biologically. Chemical synthesis involve the use of two or more precursor chemicals, which render the process toxic, expensive, and energy-intensive (Sufyan et al., 2021). However, biological methods using plant extracts (green synthesis) as reducing and capping agents, attributed on their phytochemical compounds offer a more economical, sustainable, and environmentally friendly approach to producing metal oxide nanoparticles. In addition, green synthesis results in the production of well-dispersed and stabilized nanoparticles with varying morphologies fit for various applications.(Faisal et al., 2021).

In this study, zinc nitrate hex hydrate (Zn $(NO_3)_2$) was reduced to ZnO NPs by a green technique using *Erythrin*a *abyssinica* stem bark extracts. The resulting ZnO NPs were then used as photo- anode. *Erythrina abyssinica* stem bark contains phytochemical compounds such as alkaloids, saponins, phenolics (flavonoids), tannins, and terpenoids, which are essential in the green synthesis of metal oxides (Faisal et al., 2021). The structural, morphology, and optical properties of ZnO as a photo-anode in DSSCs were investigated in this work.

1.2 Problem Statement

Dye-sensitized solar cells (DSSC) belong to the third generation of solar cell .A DSSC's power conversion efficiency is largely dependent on effectiveness of light harvesting, transfer of charge, and recombination (Magiswaran et al., 2021). The structure and morphology of photo- anode materials is directly related to those parameters. However, the low electron mobility (0.1-4 $cm^2V^{-1}s^{-1}$) of titanium

dioxide found in the majority of DSSCs that use it as a photo- anode limits their ability to perform. The chemical stability, better electron mobility (100-2000 $cm^2V^{-1}s^{-1}$) hence better electrical conductivity of the nontoxic and cheaper zinc oxide nanoparticles green synthesized from *Erythrina abyssinica* stem bark extracts relative to titanium dioxide, and durability against photo corrosion make it a potential alternative to titanium dioxide for the photo anode in DSSC.

1.3 Objectives of the Study

1.3.1 Main Objective

To investigate the power conversion efficiency of a dye sensitized solar cell fabricated using green synthesized zinc oxide nanoparticles as photo-anode.

1.3.2 Specific Objectives

(i) To determine the crystalline structure of zinc oxide nanoparticles synthesized from *Erythrina abyssinica* stem bark extracts.

(ii) To determine the average size of zinc oxide nanoparticles.

(iii) To determine the optical properties of zinc oxide nanoparticles.

1.4 Significance of the Study

The study will guide other researchers to make a dye-sensitized solar cell for study purposes in the world. The information obtained will help in achieving the national development plan of universal access to electricity. The knowledge acquired will help fulfill sustainable Development Goal No.7, of United Nations (UN), which is to guarantee that everyone has access to modern, affordable, reliable and Sustainable energy by 2030.

1.5 Scope of the Study

The photo-electrode made of zinc oxide was the main focus of this investigation. Using the green synthesis method, Zinc oxide nanoparticles were synthesized from *Erythrina abyssinica* stem bark extracts. After that the produced Zinc Oxide nanoparticles (ZnO NPs) were used as photo-anode in the dye-sensitized solar cell (DSSC).

CHAPTER TWO: LITERATURE REVIEW

2.1 Introduction

The findings by the past writers in line with this study are presented in this chapter. Solar cell, Dye sensitized solar cell, Taxonomy, morphology, propagation and uses of *Erythrina abyssinica*, Factors influencing synthesis of zinc oxide nanoparticles (ZnO NPs), Mechanism of green synthesis of ZnO NPs, synthesis of ZnO NPs and Characterization techniques have been covered.

2.2 Solar Cell

A solar cell is a PV device which uses photovoltaic effect in converting solar radiation to electric liveliness. The bending of the bands at the p-n junction Figure 2.1 leads to absorption of the photons at the p-n junction generating electron-hole pairs.

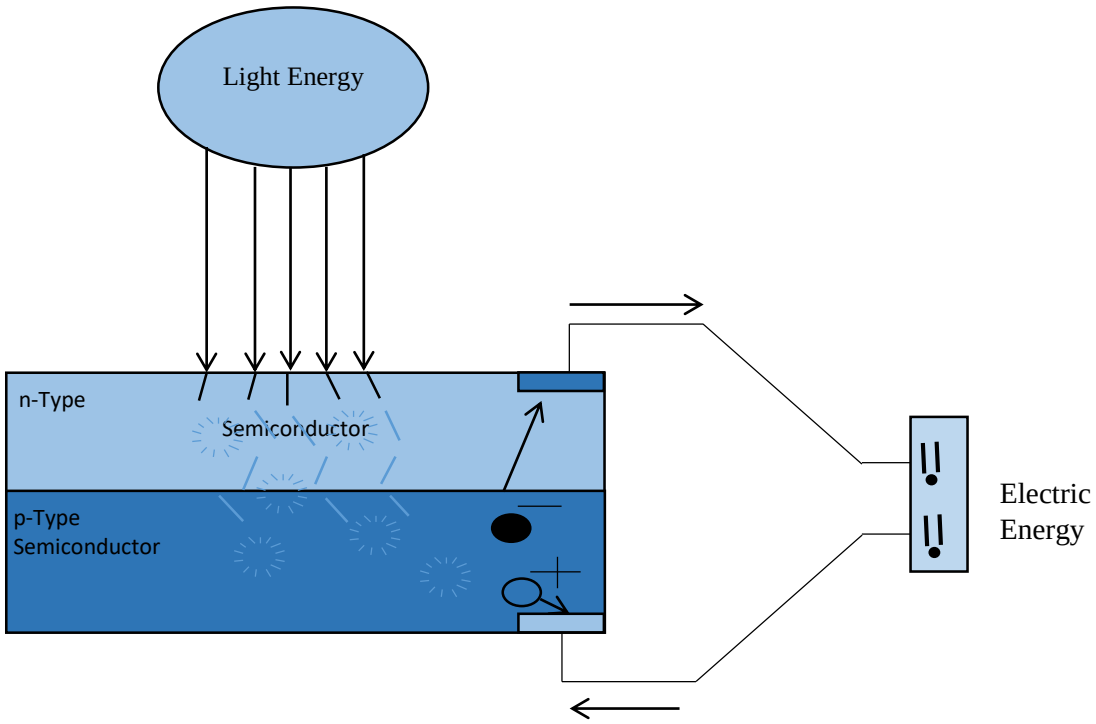

Figure 2. 1*: Structure of a solar cell* (Sharma et al., 2018)

The internal electric field at the junction helps to separate electron hole pairs generated as a result of photon absorption, resulting in power generation.

2.3 Dye-sensitized Solar Cell (DSSC)

A DSSC consists of a thin-layer solar cell Figure (2.2) which is developed by arranging two glass, transparent conducting oxide (TCO) electrodes (Sharma et al., 2018).

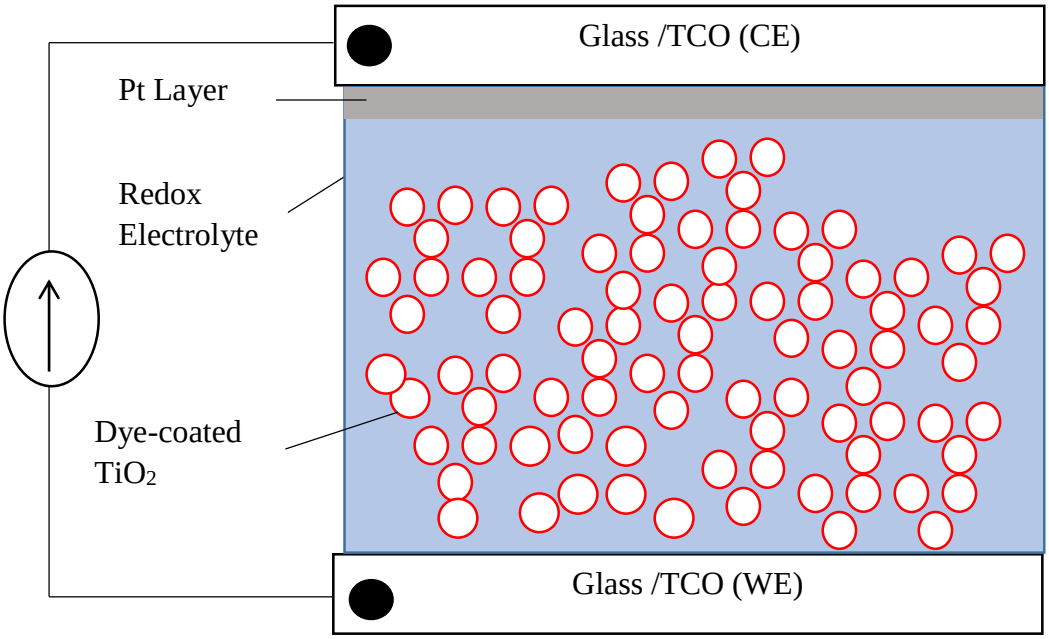

Figure 2. 2: Dye-sensitized solar cell (DSSC) (Sharma et al., 2018)

The photo sensitizer is coated on the working electrode (WE) and the second TCO is coated with a counter electrode made of finely split platinum. A mixture of iodide and triiodide-containing organic electrolyte fills the interlayer gap.

2.3.1 Power Generation by Dye-sensitized Solar Cell

When the cell is illuminated, electrons that are photo excited move from the lower (ground) state of the dye to higher (excited) state (Figure 2.3)) (Sharma et al., 2018). Charge transfer then occurs into the titanium dioxide's conduction band.

Then, electrons from the anode exit the TiO_2 hence completing the circuit to the external load thus generating electricity

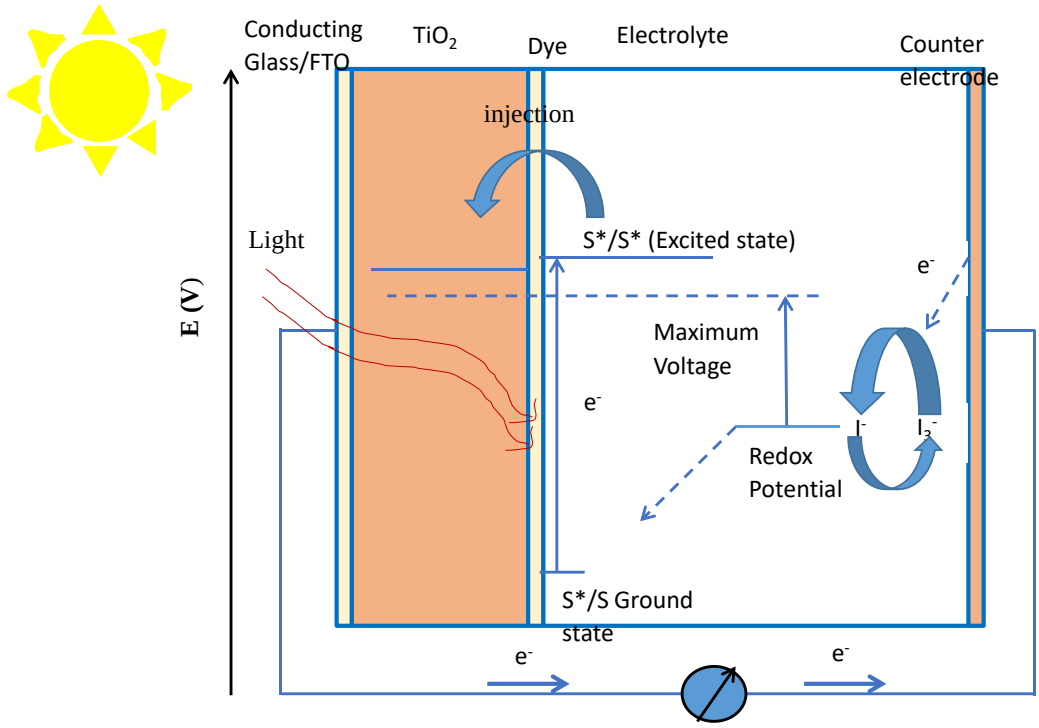

Figure 2. 3: Structure and mechanism of power generation by DSSC(Sharma et al., 2018)

When electrons get into the electrolyte on the counter electrode (CE), triiodide ions are converted into iodide ions. Iodide ions diffuse through the solution until they reach the dye, where they lose their electrons and oxidize to generate triiodide ions. Power is generated by the repetitive irradiation of light (Asahi et al., 2022).

2.3.2 Parameters of a DSSC

1. Short-circuit current density (J_{sc}), J_{sc} describes the ability of the cell to perform. It shows the highest value of current produced by cell when it not connected to any external circuit and being exposed to the maximum amount of light (Vittal & Ho, 2017).

Jsc increases when dye molecules absorb more light in a cell. Ion pairs are created when photons from incident light are absorbed by the dye or any sensitizing material, hence more photo current. The higher the $J_{sc,}$ the more absorption occurs. and the more effectively absorbed photons are converted into electron -hole pairs. As light intensity increases, the J_{sc} rises. Its unit is amperes per square centimeter (Acm^{-2}) (Vittal & Ho, 2017).

2. Open circuit voltage (V_{oc}). This describes the p.d across the cell when no external load is connected the cell. It represents the voltage across the cell's terminals in absence of an external load. The greatest voltage that the DSSC may produce when operating in an open circuit is known as $V_{oc.}$. The potential for the DSSC to produce high voltage resulting into more electricity more is indicated by a higher V_{oc} (Vittal & Ho, 2017).

3. Fill factor (FF). The fill factor describes quantity and effectiveness of the electric power produced by the cell. It can be expressed as a percentage or decimal. The effectiveness with which the DSSC transforms light to electric power is indicated by the fill factor. The fill factor is determined equation 2.1 (Asahi et al., 2022). The is the product of the maximum current and the maximum voltage (V_{max}) multiplied by the maximum current (J_{max}) gives the maximum power output as seen in equation 2.1. The open-circuit voltage (V_{oc}) multiplied by short-circuit current density (Jsc) is the P_{theory}.

$$FF = \frac{Pmax}{Ptheory} = \frac{Vmax\ Jmax}{Jsc\ Voc} \qquad (2.1)$$

4. Power conversion efficiency (η or PCE). PCE or η of the cell describes the mount of the electrical power produced by the cell, η is obtained as a percentage and it shows how the cell captures solar energy and convert it electrical power. It

is determined by considering variables such as, Jsc, V_{oc} and FF plus power input. The η of a DSSC is calculated using equation 2.2 (Deepa et al., 2012).

$$\text{PCE} = \frac{Pmax}{Pin} = \frac{Jsc\ Voc\ FF}{Pin} \quad (2.2)$$

Where P_{in} is the incident power from sunlight, which is commonly expressed in Watts per square meter (Wm^{-2}) and is the total amount of solar energy falling on the DSSC.

2.4 Taxonomy, morphology and propagation of Erythrina abyssinica

The genus *Erythrina,* the phylum spermatophyte, the class magnoliopsida, Order Fables, the family Fabaceae, the sub family Papilionoidea, the kingdom Plantae and the species *abyssinica* , are descriptions of the plant (Aerts, 2008).

Erythrina abyssinica can reach a height of 12 to15m a multibranched deciduous tree shrub tall (Figure 2.4). leaves are trifoliate with alternate arrangement and abundant hair, typically at the surface and long hairy spherical leaves. Rounded leaves are seen at the base, obtuse or notched at the apex. It has corolla flowers with free kneel petals that are colored (orange to red), ten petals that are fused and 1stamen that is free (Kone et al., 2011).

The fruits are rectangular, linear pods that range in color from, brown to black. The tree has deep roots in the ground that keeps it firm. Cuttings or seeds are used when propagating this plant. It grows naturally in wood lands and grass lands.

Figure 2. 4: Erythrina Abyssinica plant (photo taken by Balabye Stephen from Matuba village Mayuge district)

2.4.1 Uses of *Erythrina Abyssinica*

As a legume *Erythrina abyssinica* is widely known for improving soil fertility by fixing nitrogen into the soil. As a result, it is crucial for forest regeneration and Phyto restoration in polluted soils (Abebe Abay, 2018) .It is important in agriculture because its flowers also release nectar that pollinating insects especially bees feed on. It also produces a substance used in making dye and craft materials like necklaces from seeds. Additionally, the stem of this plant is harvested for charcoal and timber ,which are used for energy and furniture in turn (Aerts, 2008). The most often utilized part in the manufacture of herbal treatments are the stem bark and roots. Roots and stem bark have been extensively studied, even in phytochemical research (Korir et al., 2011).

Leprosy, malaria, bacterial and fungal infections are some of the commonly reported illness that are treated using *Erythrina* a*byssinica.* Inflammatory diseases, Tuberculosis snake bite, antagonizing poisons, sexually transmitted diseases (Shaba et al., 2021), urinary tract infections, skin infections, diarrhea, infertility, epilepsy, vomiting, hepatitis and helminthiasis are among the other ailments this

herb treats (Abebe Abay, 2018).Poultry livestock diseases such as new castle can be treated using extracts of *Erythrina abyssinica* (Shaba et al., 2021)

Different solvent extracts of Erythrina abyssinica contain phytochemicals such as alkanoids, Flavanols, flavonoids which can reduce metal salt solutions to metal ions (Abebe Abay, 2018). Because of its vibrant colors, some communities raise this plant in their home steads as an attractive plant for live fencing, even though it typically grows originally in the wild (Aerts, 2008).

2.5 Factors Influencing the Synthesis of Zinc Oxide Nanoparticles

1. PH in the mixture reaction. The type of ZnO nanoparticles is determined by the reaction mixture's PH (Sangeetha et al., 2011)**.** The electrical charge of molecules is changed by the PH of the solution, and this charge will impact their decrease. Hydroxyl ions (OH^{-1}) are usually few during the synthesis of ZnO in acidic solution (PH less than 7) which hinders the hydrolysis and condensation process. Since the hydrogen and hydroxyl ions are equivalent at the PH of 7 (neutral), little or no effect is observed on the surfaces of crystals. When the PH in the mixture of reaction is more than 7, hydroxyl ions increase in number and attraction of zinc ions with hydroxyl ions strengthens (Sangeetha et al., 2011). Zinc hydroxide and other intermediate products are created when hydroxyl ions are present in a solution at high concentrations.

2. Concentration of precursors and capping agents

Capping agents are responsible for controlling the growth rate, size of the particle, and preventing aggregating of particle (Sangeetha et al., 2011).The size of the crystallite of ZnO NPs increases when the zinc salt precursors' concentration is increased.

3. Reaction temperature.

An increase in reaction rate at higher temperatures leads to increasing reaction rate in ions of the metal and creation of smaller NPs (Sangeetha et al., 2011)**.** . Zinc ions are rapidly reduced by raising the reaction temperature, Which leads to the creation of ZnO NPs with decreasing crystallite sizes (Kumar et al., 2013).

4. Time of reaction. It refers to the time that is needed to complete all steps; that is to say reducing and forming new particles. NPs start forming within minutes after adding metal salt precursors (Syed Zahirullah et al., 2018).

2.6 Mechanism of Green Synthesis of Zinc Oxide Nanoparticles

Extracts of the Plant contain phytol chemicals such as phenolic compounds that can reduce zinc nitrate hexahydrate to metal nanoparticles (Cauda et al., 2014). The phytol chemicals are antioxidant and non- toxic, hence they can reduce and stabilize substances. These phytol chemicals change at varying concentrations in different extracts of the plant types (Subramanian & Al, 2013). The composition of the leaf extract significantly affects nanoparticle synthesis and quality of nanoparticles produced (Shokry Hassan et al., 2014). There are three steps for stabilization of metal ions after the plant extracts have been reduced.

Activating phase. In the activating phase, metal ions are reduced and nucleation of metal atoms that have been reduced takes place.

Growing phase; in the growing phase, stability of nanoparticles is involved, small adjacent nanoparticles combine into particles of large size, this is accompanied by the stability of nanoparticles. The more the growth phase, the more the nanoparticles blend forming nanowires.

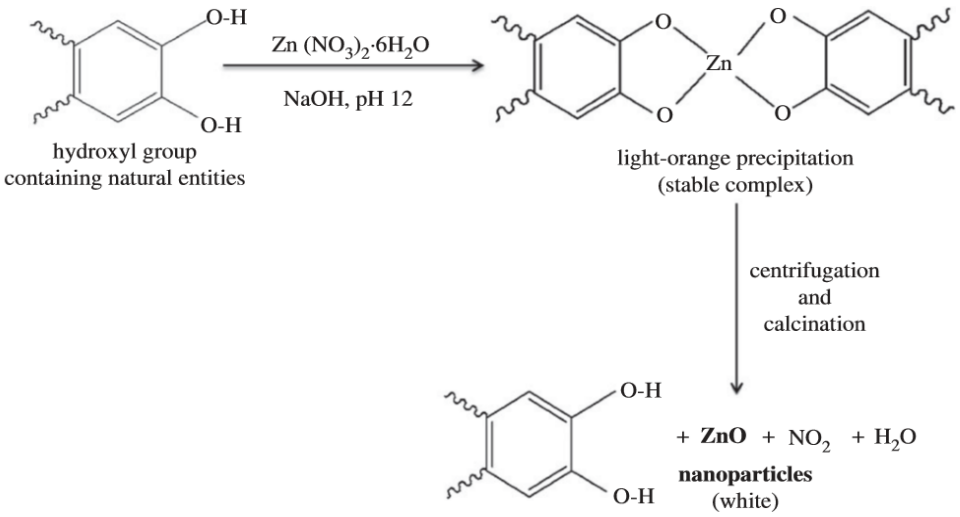

Figure 2. 5: Mechanism of green synthesis of ZnO nanoparticles

3 Terminating phase; consisting of shape of nanoparticles formed; in the terminating phase, the nanoparticle size and shape can be confirmed. The ability of plant extracts to stabilize metal nanoparticles has a great impact on this process. Metal ions reach the growth and stabilization phase through the action of phytol chemicals. Ultimately, Oxygen formation leads to metal ion bonding and formation of a distinct shape. (Basnet et al., 2018).

2.6.1 Zinc Oxide Nanostructures

Three crystal structures, of zinc oxide are shown, wurtzite, Figure 2.6 (a), zinc blende, Figure 2.6 (b), and rock salt, Figure 2.6 (c). Wurtzite is the most stable structure. Zinc blende formation is as a result of zinc oxide growing on the substrate in a proper cubic lattice, and the rock salt structure is obtained at relatively high-pressure synthesis. Zinc (Zn) and oxygen atoms are joined at tetrahedral sites in alternating configuration to form the hexagonal closely packed Wurtzite structure (Cauda et al., 2014).

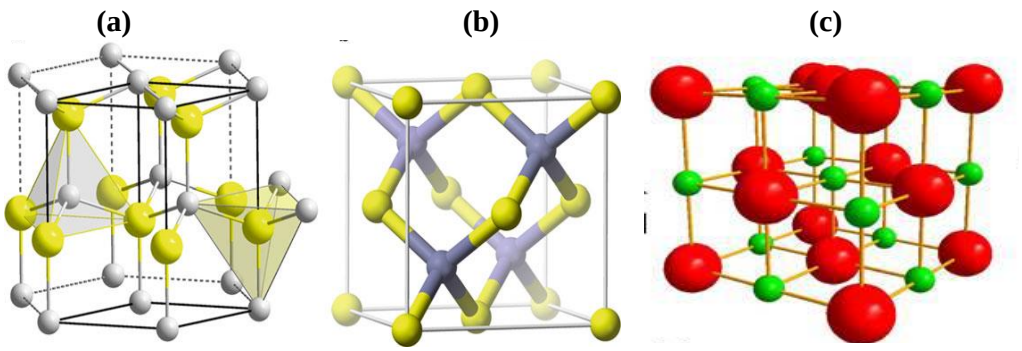

Figure 2. 6: ZnO crystal structures; (a) wurtzite; (b) zinc blende; (c) rock salt (Shaba et al., 2021)

According to (Shashanka et al., 2020),ZnO is an n-type semiconductor material with favorable optical and electrical properties. Its high electron mobility, high thermal conductivity, the wide band gap (3.37 eV) in comparison to titanium dioxide ((3.20 eV) which sustains a large electric field and large excitation binding energy (60 meV) (Li et al., 1997) are responsible for its good optical and electrical properties. Zinc oxide has UV absorption between 200 and 300 nm and near-visible emission between 500 and 600 nm (Hong et al., 2009).

2.7 Synthesis of Zinc Oxide Nanoparticles

3 g of ethylene glycol and one gram each of urea and zinc acetate hydrate were mixed in a bowl. A magnetic stirrer was used to agitate the mixture for one hour. To evaporate the solvent, the mixture was put in a domestic micro wave oven. To remove un wanted water-soluble chemicals and organic compounds present in the sample, the substance deposited in the bowl was removed and washed four times using acetone and double distilled water. The synthesized zinc oxide NPs were filtered, dried in a hot air oven at 80 ^{o} C for 4 hours, and annealed in a muffle furnace at 500 ^{o} C for two hours To increase the sample's crystallinity, the produced zinc oxide nanoparticles were filtered, dried for four hours at 80 ^{o}C in a

hot air oven, and then annealed for two hours at 500 ^{o} C in a muffle furnace (Esakki et al., 2021).

2.8 Characterization of Zinc Oxide Nanoparticles

The surface morphology, as well as the optical and structural characterization of ZnO NPs, are the topics of this discussion. Utilizing plant extraction to produce high-quality zinc oxide nanoparticles requires careful characterization.

UV-visible spectroscopy, scanning electron microscopy, X-diffractogram, energy dispersive spectrometry, and Fourier-Transform-Infrared spectroscopy were all used to characterize zinc oxide.

From the absorption spectra of nanoparticles that were synthesized at different concentrations and temperatures the optical property of generated zinc oxide nanoparticles was discovered (Rahman et al., 2022). At 320 nm, there was an absorption peak. The biosynthesized images of zinc oxide nanoparticles were taken using Nova nano scanning electron microscope with accelerating voltage of 10 kilovolts. The characterization showed that zinc oxide nanoparticles were present in its agglomerated form (Sha et al., 2022).The crystalline material was analyzed by XRD, with wave-length 1.5406 angstrom (Å) of copper k-alpha radiation. From the X-diffractogram pattern analysis 51.24 nm as average size of nanoparticles was estimated (Shokry Hassan et al., 2014). The energy dispersive spectroscopy was used to determine nanoparticle elemental composition. From the results zinc showed a composition of strong signal at 78.32 % and oxygen showed a strong signal composition of 12.78 %. (Lin et al., 2016).

CHAPTER THREE: MATERIALS AND METHODS

3.1 Introduction

This chapter discusses the research design, Chemicals and materials used, preparations of plant extracts, synthesis of zinc oxide nanoparticles, Dye preparation, Development of zinc oxide thin films on Fluorine-doped tin oxide (FTO) substrate and dye adsorption, Development of platinum on FTO substrate, Preparations of liquid electrolyte, Characterization of thin films and ZnO, Determination of optical properties of Ruthenium dye N719, Fabrication and testing of a DSSC.

3.2 Research Design

This study involved experimental method of collecting data. Figure 3.1 shows a summary of key processes involved before the fabrication of the DSSC. The data obtained was analyzed using Origin 24 software (Kishore Kumar et al., 2020).

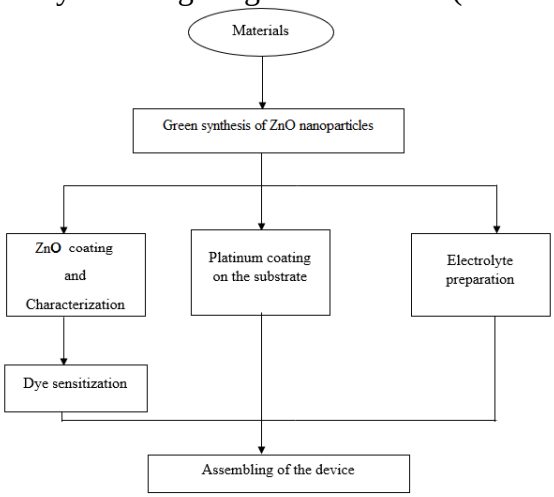

Figure 3. 1: Research design

3.3 Chemicals and Materials

The chemicals plus materials which were used to synthesize zinc oxide nanoparticles were zinc nitrate hexahydrate, ethanol, hexachloroplatinic powder, *Erythrina abissinica* stem barks obtained from Matuba village Mayuge District,

distilled water, oven, grinder, analytical balance, measuring cylinder, centrifuge, Whatmanfilter paper, Fluorine-doped tin oxide (FTO) substrates. Platinum was used as CE and zinc oxide as photo anode. Iodide /triiodide was used as the electrolyte. The other materials included multimeter, mobile pipette, furnace, binder clips. All chemicals were obtained from Sigma Aldrich.

3.4 Preparation of Plant Extracts

Erythrina abyssinica stem barks were collected, cleaned well using distilled water to remove dirt and other particles. The stem barks were then dried at room temperature after being them washed. 30.0 g of the stem bark were weighed, cut into small slices and ground to form fine powder.

3.5 Synthesis of Zinc Oxide Nanoparticles

5 g of the powder were dissolved in 100 mL of distilled water, heated at 70 ^{0}C on a magnetic stirrer (Rahman et al., 2022) for 15 minutes to soften the cell membrane followed by filtering to remove loose particles and then put in a centrifuge for 10 minutes at 2400 rpm at room temperature, and then decanted. The filtrate was mixed in 5.0 g of zinc nitrate hex hydrate and again heated under constant magnetic stirring at 70 ^{0}C (to increase the rate of chemical reaction) for 15 minutes (Rahman et al., 2022) The solution was put in an oven at 120 ^{o}C and left there overnight.

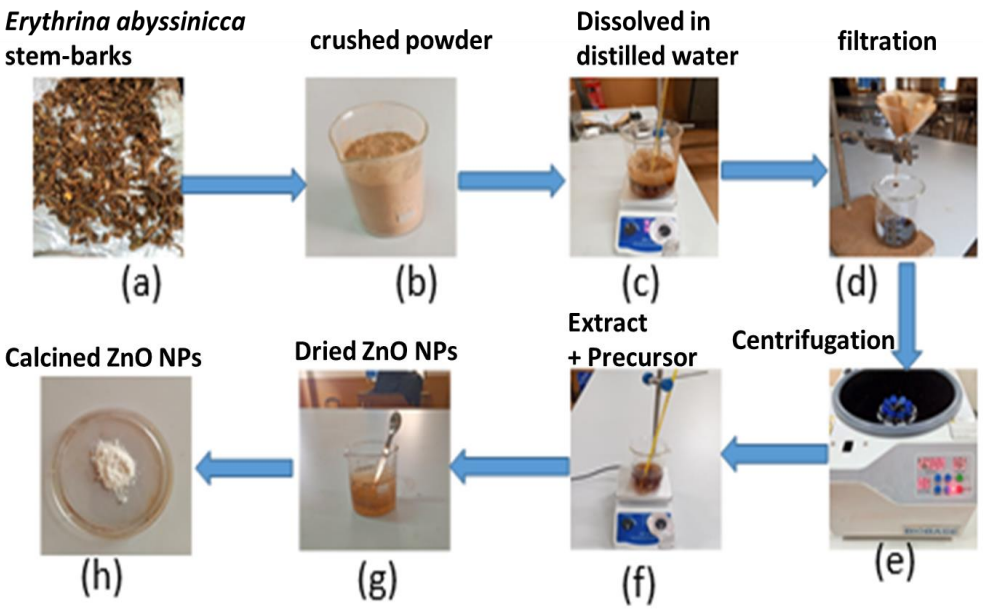

Figure 3. 2: Synthesis of Zinc oxide nanoparticles

The bonded particles were crushed and then annealed in a furnace, one sample after the other at 300 ° C, 400 ° C, 500 °C and 700 ° C for two hours (Subramanian & Al, 2013).

3.6 Dye Preparation

20 ml of ethanol were used to dissolve 10 mg of Ruthenium dye (N719) (Shashanka et al., 2020). After 2 hours of stirring, at room temperature, the solution was stored in a dark bottle for later use (Charbonneau et al., 2010).

3.7 Development of ZnO Thin Films on FTO Substrate and Dye Adsorption

De-ionized (DI) water and ethanol were used to thoroughly clean the FTO glass substrates. It was sonicated for three hours in a mixture containing DI and ethanol. In a 0.4 g of polyethylene glycol with a solution of glacial acetic acid and 5 ml of double distilled water each, 1g of ZnO nanopawder was dissolved (Rahman et al., 2022). The resultant mixture was placed in an ultrasonic bath for 2 hours. The edges of FTO substrates were sealed using cello tape. ZnO paste was drop casted

on the substrate using a 200 micro pipette and kept for 24 hours before annealing at 300 ^{o} C in a furnace for 1 hour (Zhang et al., 2020). The film was put in the dye extract for 24 hours. The soaked film was removed from the dye, rinsed with ethanol and then used as photo-anode (Esakki et al., 2021).

3.8 Development of Platinum on FTO Substrate (Counter Electrode)

2 mg of hex platinic powder was dispersed in 1 ml of ethanol (Ito et al., 2008) and the solution was stirred for 15 minutes (Afaq et al., 2018). The solution was drop casted on a pre-cleaned FTO glass substrate using a 200-micro pipette. The sample was kept for 24 hours to evaporate the solvent room temperature before annealing at 400 ^{o} C for 15minutes (Yeh et al., 2015).

3.9 Preparation of Liquid Electrolyte

In a clean beaker 10 ml of ethylene glycol was used to dissolve 0.127g of iodine and 0.83 g of potassium iodide (Esakki et al., 2021). The mixture was stirred for 30 minutes using glass rod and stored in a sealed bottle (Nuran et al., 2015).

3.10 Characterization of Thin Films and ZnO

The crystalline structure, lattice parameters of green synthesized ZnO nanoparticles (ZnO Nps) were investigated using SHIMADZU XRD-700 X-ray diffractometer at an irradiation wave length of 1.5406 Å copper k-alpha (Cuk_{α}). The elemental composition of the ZnO Nps was determined using Energy Dispersive X-ray Spectroscopy. The surface morphology examination and average particle size of ZnO Nps was obtained using Gemini 1 ZEISS Scanning electron microscope (SEM) (Subramanian & Al, 2013). Ultra Violet-Visible (UV-vis) spectroscopy was carried out to find the optical properties by the help of an ultra violet UV-vis Speedo photometer in Diffuse Reflectance Spectroscopy (DRS)

mode from which the absorption and reflection spectra of the green synthesized ZnO Nps were obtained.

3.11 Determination of Optical Properties of Ruthenium Dye N719

An ultra violet visible spectrophotometer was used to determine the optical properties of ruthenium dye N719. This was used because dye molecules have characteristic absorption bands ranging from ultra violet to visible regions of the electromagnetic spectrum. Two cuvettes, one containing dye solution and the other having solvent were inserted in the sample compartment of the spectrophotometer as shown in Figure 3.3. A beam from Ultra violet visible light source was allowed to hit a monochromatic so that abeam of single wave length pass through it. It was divided into two intensity beams using a half-mirrored device.

Figure 3. 3: UV-Visible spectrophotometer (Photo was taken from the Chemistry laboratory of Kyambogo University)

One beam went through a cuvette having sample a solution of the under investigation and the other passed through a similar cuvette having only the solvent. The resultant intensities of the light beams were then measured using

spectrophotometer and a comparison was made. The resulting spectra were analyzed using origin soft ware (Kishore Kumar et al., 2020) and then used to determine optical properties of the sample.

3.12 Fabrication and Testing of the DSSC

The adsorbed dye on ZnO electrode and platinum counter electrode were sandwiched with conductive sides facing each other. The electrolyte solution was dropped at the edges of the substrate and drawn into space between the electrodes by capillary. Binder clips were used to hold the electrodes together as seen in Figure 3.4 (d). The cell's performance was measured from a solar simulator under one- sun illumination Figure 3.4 (e)

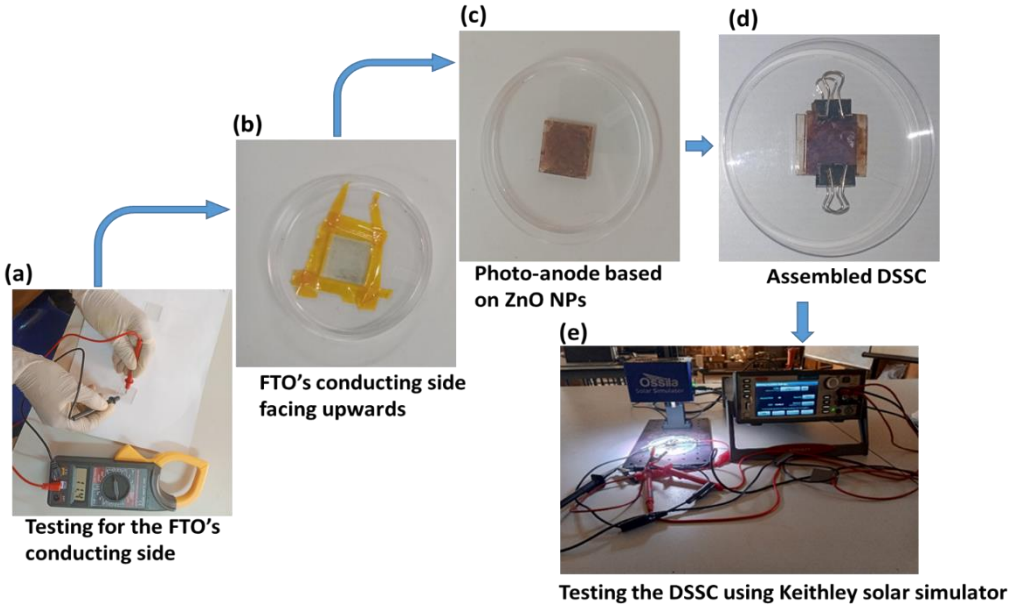

Figure 3. 4: Fabrication and testing of the DSSC

The fabricated cell was connected to Keithley SMU-2450 using four probe and then placed below the solar simulator where by the photo anode faces the lamp of the solar simulator. The sweep and stop voltages of Keithley were set at -1V and +1V respectively.

The Keithley was then triggered to generate a graph and the data was used in origin to produce current-voltage (I-V) and power- voltage (P-V) characteristic curves of the cell.

CHAPTER FOUR: RESULTS AND DISCUSSION

4.1 Introduction

The chapter discusses structural analysis of ZnO nanoparticles, the examination of ZnO NPs using Scanning electron microscopy, Optical properties of the synthesized ZnO NPS and power conversion efficiency of the Dye-sensitized solar cell using zinc oxide as photo-anode.

4.2 Structural Analysis of ZnO Nanoparticles

Figure 4.1(a) shows the XRD pattern of ZnO NPs, this pattern agrees with the space group $P6_3mc$ (JCPDS number 00-036-1451), the standard pattern. The XRD confirmed the Wurtzite structure (hexagonal phase) of ZnO NPs. The diffraction peaks at 2θ = 31.67, 34.35, 36.16, 47.47, 56.52, 62.82, 66.31, 67.90, 69.03, 72.54, and 76.92º correspond to diffraction planes of (100), (002), (101), (102), (110), (103), (200), (112), (210), (004), and (202) respectively as shown in Figure 4.1 (a). The extra peak at 28.30º marked as (*) at temperatures of 300, 400, and 500 ℃ was due to the impurity phase of $Zn(OH)_2$ in ZnO. It was found out that this impurity peak decreased until it disappeared at 700 ℃. The full width at half maximum (FWHM) in the XRD study was shown to decrease as the calcination temperature rose resulting in sharper, smaller peaks with higher intensities at higher temperatures. Thus, highly crystalline and pure ZnO NPs were obtained. At 700 ℃, very crystalline and pure ZnO NPs were thus produced, and further investigations revealed a similar pattern.

Table 4. 1: Results from XRD

Peak No	Peak position (2θ)	β (300 ° C)	β (400 ° C)	β (500 ° C)	β (700 ° C)	Miller indices
1	31.7	0.69546	0.58618	0.44543	0.23309	100
2	34.4	0.69555	0.58642	0.44557	0.23294	002

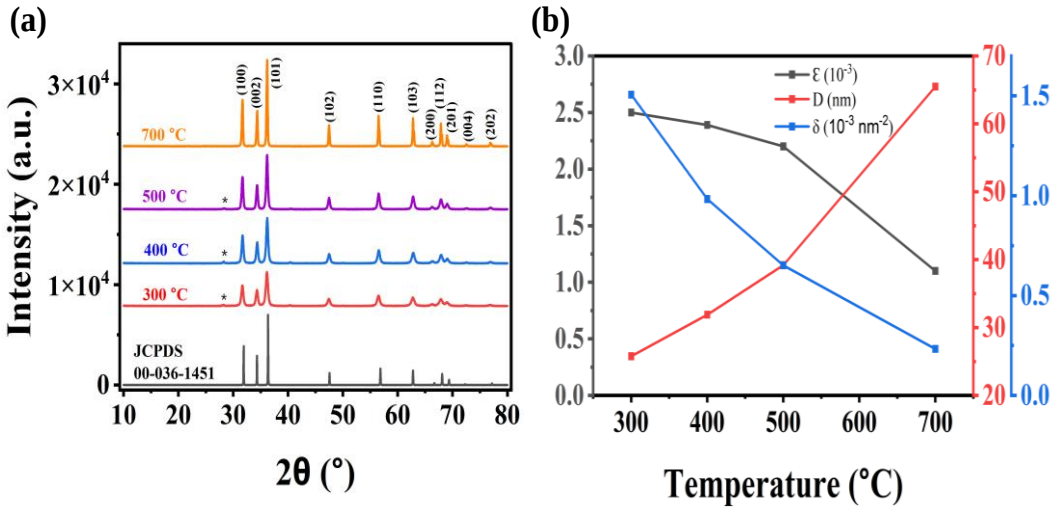

Figure 4. 1: (a) XRD pattern of bio-synthesized ZnO Nps and (b) variation of average particle size (D), micro strain (ε) and dislocation density (δ)with temperature.

4.2.1 Determination of lattice parameters

An impact on lattice strain and crystallite size (D) on diffraction peak's widening can be represented by the Williamson–Hall (W–H) equation (4.1).

$$\beta_{hkl} \cos\theta = \frac{K\lambda}{D} + 4\varepsilon \sin\theta \qquad (4.1)$$

K is a constant (0.9) according to the shape, λ is the wave length (1.5406 Å), θ is the angle of diffraction, β_{hkl} is the peak broadening at full width half maximum (FWHM) corresponding to plane of diffraction (*hkl*), D is the crystallite size and ε is the micro-strain (Pandey et al., 2016). The size of the crystal and micro-strain can be obtained. $(\frac{K\lambda}{D})$ as an intercept and ε as the slope can be obtained from the

W–H plot of $\beta_{hkl}\cos\theta$ against $4\sin\theta$ in which the size of the crystal and micro strain respectively can be determined. The dislocation densities, δ, of the samples were calculated using equations 4.2 (Pandey et al., 2016)

$$\delta = \frac{1}{D^2} \tag{4.2}$$

As shown in Table 4.2, the average crystallite size increases when calcination temperature increases. As calcination temperature is increased, migration of grain boundaries occur, causing the coalescence of small grains and formation of large grains (Pandey et al., 2016).

The lattice parameters a and c were respectively calculated from Equations (4.3 and 4.4) for the annealed ZnO at 300, 400, 500 and 700 ^{o} C.

$$a = \frac{\lambda}{\sqrt{3}\sin\theta} \tag{4.3}$$

$$c = \frac{\lambda}{\sin\theta} \tag{4.4}$$

However, for hexagonal structure, a is equal to b hence a = 3.26 Å, $b = 3.26$ Å and $c = 5.21$ Å.

The interplanar spacing d_{hkl} was obtained from the relation; $a = d_{hkl}$ (Bindu & Thomas, 2014), $d =$ 3.26 Å. The lattice angles were α=90 ^{o}, β=90 ^{o} and γ= 120 ^{o}.

Table 4. 2: Calculated average crystallite size, micro-strain, dislocation density, and lattice constants of ZnO NPs

T (°C)	D (nm)	Ɛ	δ (nm^{-2})	Lattice Constants	
				a (Å)	c (Å)
300	25.8	0.0025	0.00151	3.2627	5.2124
400	31.9	0.0024	0.00098	3.2597	5.2128
500	39.2	0.0022	0.00065	3.2577	5.2135
700	65.5	0.0011	0.00023	3.2568	5.2138

Table 4.2 shows increased crystallite size from 25.8 to 65.5 nm with an increase in the calcination temperatures of the ZnONPs This is attributed to the growth of particles as a result of an interfacial reaction. The dislocation densities and micro-strain both decreased with a rise in the calcination temperature, as shown in Figure 4.1(b). This means that the lattice defects gradually diminished, and led to improved crystallinity of ZnO NPs at the higher temperature. The calculated lattice constants for the bio-synthesized ZnO NPs ranged from $a = b$ = 3.2627 Å at 300 ℃ to 3.2568 Å at 700 ℃ and c = 5.2124 Å at 300 ℃ to 5.2138 Å at 700 ℃ as indicated in Table 4.2. As the calcination temperature was increased there was a significant decrease in lattice parameter *a* with a slight increase in lattice parameter *c*, which in turn led to a reduction in the volume of the unit cell. The increase in temperature resulted in a more structured arrangement of crystals within the lattice, featuring fewer impurities and enhanced density, which reduced the lattice parameter. (Pandey et al., 2016).

4.3 Scanning electron microscopy analysis of the ZnO Nps

Figures 4.2 (a), (b), (c), and (d) shows the SEM images of ZnO NPs at calcination temperatures of 300, 400, 500, and 700 ℃.

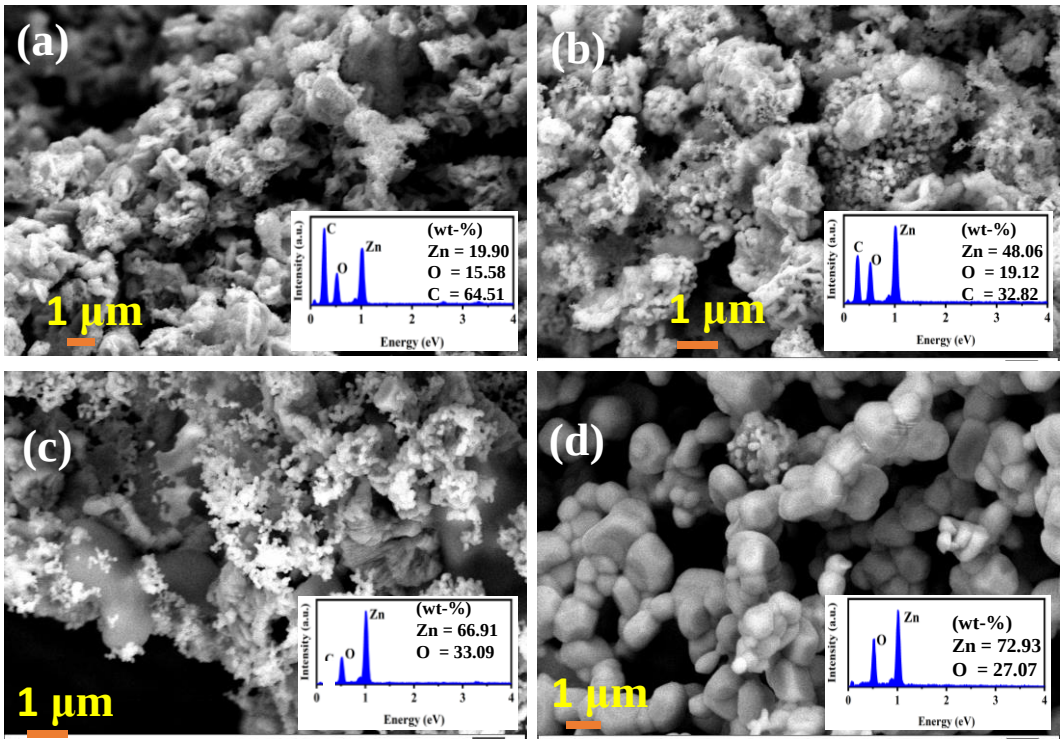

Figure 4. 2: SEM images for ZnO nanoparticles calcined at (a) 300, (b) 400, (c) 500, and (d) 700 ℃ with their respective EDX spectra (insets).

The images indicate variations in levels of agglomeration depending on the growth temperature. The micro-images in Figure 4.2 (a, b, and c) show incomplete nucleation and growth process, non-uniform, flake-like, agglomerated particles surrounding spherically shaped nanoparticles. This agglomeration is due to the polarity and electrostatic, high surface energy, van der Waals forces, or other interparticle interactions. The presence of spherical nanoparticles alongside the flake-like particles suggests a possible bimodal distribution of particle sizes and shapes. Spherical particles often form due to minimization of surface energy (Yahia et al., 2016). However, at a calcination temperature of 700 ℃, the particles become more distinguishable. This is due to the formation of larger particles at higher calcination temperatures, primarily due to grain growth and particle agglomeration. As the temperature rises, the crystallites that form get bigger and

nearby particles are more likely to fuse, creating a more compact and ordered structure as opposed to separate nanoparticle. This is consistent with the XRD results, which indicated that as the calcination temperature rose, so did the particle size. Thus, the micro-images demonstrate how temperature directly affects a material's surface shape.

ZnO NPs' elemental composition was determined using Energy Dispersive X-ray spectroscopy (EDX). The insets in Figures 4.2a, 4.2b, 4.2c, and 4.2d display the peaks and corresponding elements for each sample in the prepared ZnO NPs. EDX identified Zn, O, and C at 300 °C and 400 °C, while only Zn and O were detected at 700 °C, with wt % of 72.93% and 27.07%, respectively, indicating the formation of pure ZnO. The presence of carbon (C) likely originated from biomolecules in *Erythrina abyssinica* stem bark at 400 °C and below, which volatilized at higher calcination temperatures.

The average particle sizes, P of the spherical ZnO Nps were found to be 63 ± 2 nm ,80 ± 2 nm , 92 ± 2 and 121 ± 2 nm at 300 ^{o} C, 400 ^{o} C , 500 ^{o} C and 700 ^{o} C respectively as shown in figure 4.3 (b, d , f and e) .With increase in annealing temperature, average particle size increases, Table 4.3. The shape of particles changes from spherical to hexagonal. Increase in annealing temperature leads to an increase in length and diameter of the crystallite size (Yahia et al., 2016).

Table 4. 3: Average particle size of spherical Zinc oxide nanoparticles

Temp (^{o} C)	Particle size(nm)
300	63
400	80
500	92
700	121

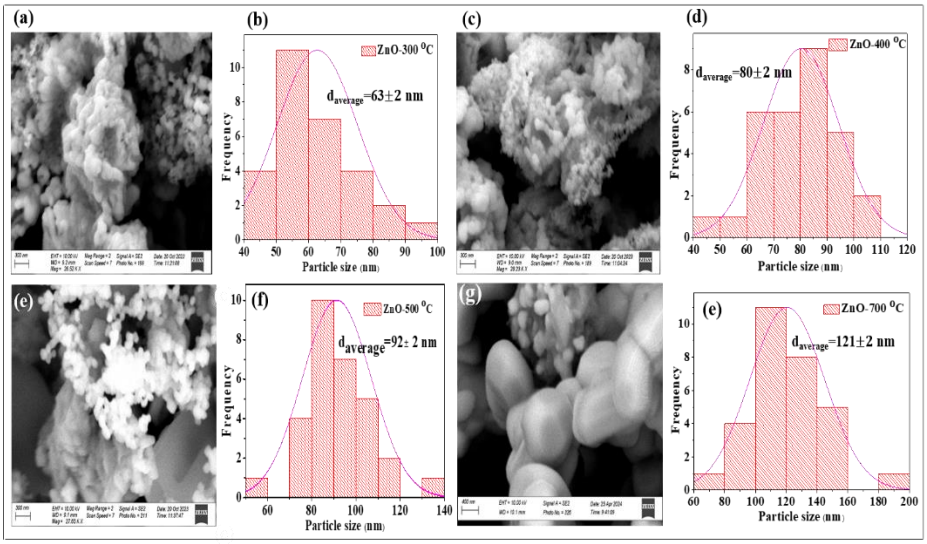

Figure 4. 3*: SEM images for ZnO Nps at synthesis temperatures of 300℃, 400℃, 500℃ and 700℃ with their corresponding histograms showing particle size distribution.*

4.4 Optical Properties of ZnO NPs

Figure 4.4 (a) shows the PL spectra of bio-synthesized ZnO nanoparticles using *Erythrina abyssinica* stem bark extract. The PL spectra of ZnO NPs at room temperature (RT) show two main emission peaks corresponding to deep level defects (DLE) and band-to-band emissions (BBE) in the visible and ultraviolet (UV) regions, respectively (Hong et al., 2009). One peak near the UV region, attributed to BBE through excitation collision processes, and a broad peak in the visible region due to deep-level emissions caused by oxygen, around 560 nm (green region) (Mansournia et al., 2015). However, it was observed that increasing the calcination temperature significantly enhanced the intensity of peaks in the blue region (420-480 nm), while the peak intensity in the UV spectrum markedly decreased. This change results from an increase in Zn vacancy defects facilitated by higher temperature, leading to prominent deep-level emissions and reduced band-to-band emissions (Cauda et al., 2014). Optical properties of the bio-

synthesized zinc oxide nanoparticles were further investigated using diffuse reflectance spectra (DRS), as shown in Figure 4.4(b). In reflection spectra, lower reflectance indicates higher absorption at the corresponding wavelength, and vice versa. The reflectance spectra for all samples are quite similar in the UV wavelength range of 310 – 377 nm. However, notable differences appear between the RT sample and those calcined at 300, 400, 500, and 700 ℃ in the visible range of 400 – 760 nm. Due to absorption of ZnO Nps at the UV region, they can be used for dye sensitized solar cell application.

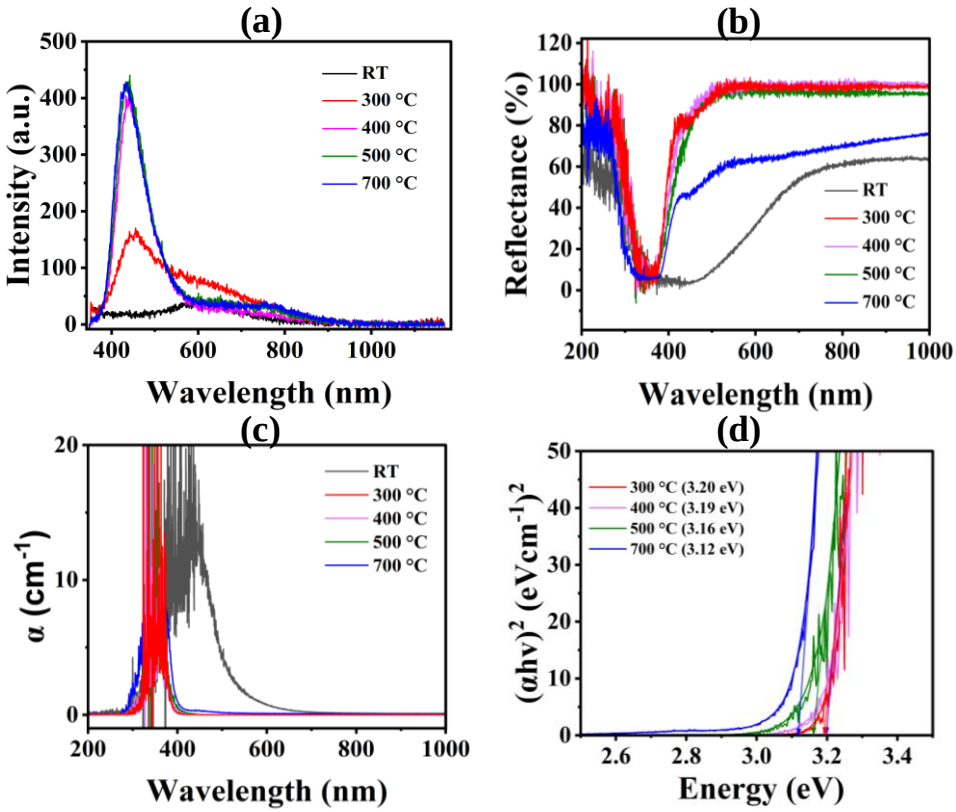

Figure 4. 4: Photoluminescence spectra of ZnO Nps (b) DRS spectra of ZnO Nps synthesized at RT, 300,400,500 and 700 0 C,(c) U.V-visible absorption spectra of ZnO Nps, and (d) Tauc plots for the synthesized ZnO Nps

4.4.1 Determination of Band Gap

The spectra from UV-vis photometer in diffuse reflectance (DRS) mode of ZnO Nps obtained by green method are shown Figure 4.4 (d). The band gap was determined from Tauc plots using equation (4.5) (Kumar et al., 2013)

$$(F(R)h\upsilon)^r = A\left(h\nu - E_g\right) \tag{4.5}$$

Where F(R) is the kubelkamunk function (Charbonneau et al., 2010) which is the ratio of absorption coefficient, to the scattering coefficient, s as seen in Equation 4.5

$$F(R) = \frac{K}{S} = \frac{(1-R)^2}{2R} \tag{4.6}$$

$h\nu$ is the energy of photon, A is a constant with respect to the material, power 2 represents direct transition and $\frac{1}{2}$ $indicates\ indirect\ transition.$

A graph of $(F(R)h\upsilon)^2$ against hυ was plotted in order to get the band gap (Kumar et al., 2013). The general equation of a straight line,$y = mx + c$,was made as a comparison to the equation (4.5) After fitting on the curves, and by linear extrapolation of the graph the band gap was obtained as seen in Figure 4.4 (d).

This value was equal to intercept value divided by the slope and is the band gap of zinc oxide nanoparticles. The optical band gap energies for ZnO nanoparticles were calculated to be 3.20 and 3.19 eV at temperatures of 300 and 400 ℃, respectively, while at temperatures of 500 and 700 ℃, 3.16 and 3.12 eV, respectively were obtained as band gaps of the optical spectra as shown in Table 4.4. These results agree with the reported 3.10 - 3.39 eV band gaps for ZnO nanoparticles (Mansournia et al., 2015).The increase in calcination temperature resulted in grain

growth with decreased defects, thus improving the crystallinity of the synthesized ZnO NPs, as supported by the SEM and XRD analysis. The ZnO NPs become less amorphous with a rise in the calcination temperature, giving a decreased band gap (Mansournia et al., 2015).

Table 4. 4: Optical band gap of ZnO Nps at different calcination temperatures

Calcination temp (^{o} C)	Band gap (eV)
300	3.20
400	3.19
500	3.16
700	3.12

4.4.2 Optical Absorption Properties of Ruthenium Dye N719

The characteristics of absorption of ruthenium dye N719 shown in Figure 4.5 indicates maximum absorbance at 384 **and** 526 nm. This shows that green and adjacent colors are absorbed and red is reflected. The absorption peak obtained is in agreement with other reports.

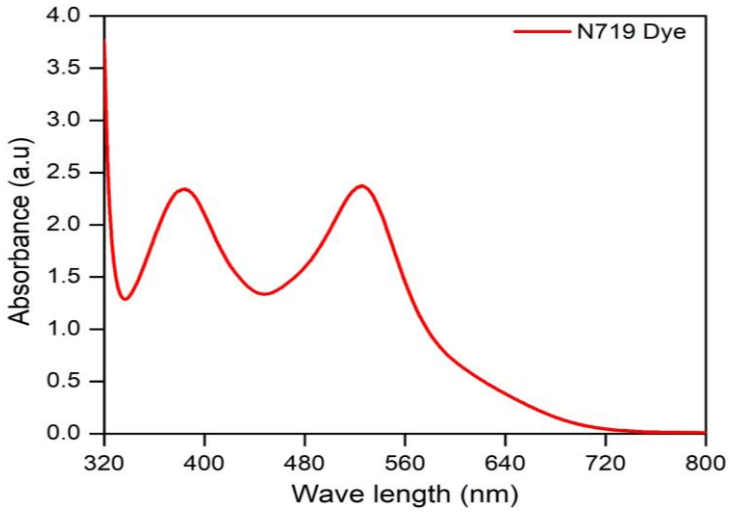

Figure 4. 5: Absorption spectra of Ruthenium Dye N719

4.5 Power Conversion Efficiency of Dye- Sensitized Solar Cell Using Zinc Oxide as Photo-Anode

Equation 4.8 was used to calculate the fabricated DSSC's power conversion efficiency. To examine the power conversion efficiency of the fabricated DSSC, Photo current density (J) versus voltage (V) curve under a simulated illumination with the light intensity of 100 mW/cm^2 was observed. Figure 4.6 (a, b) shows the typical J-V curve and power density curve of the fabricated DSSC.

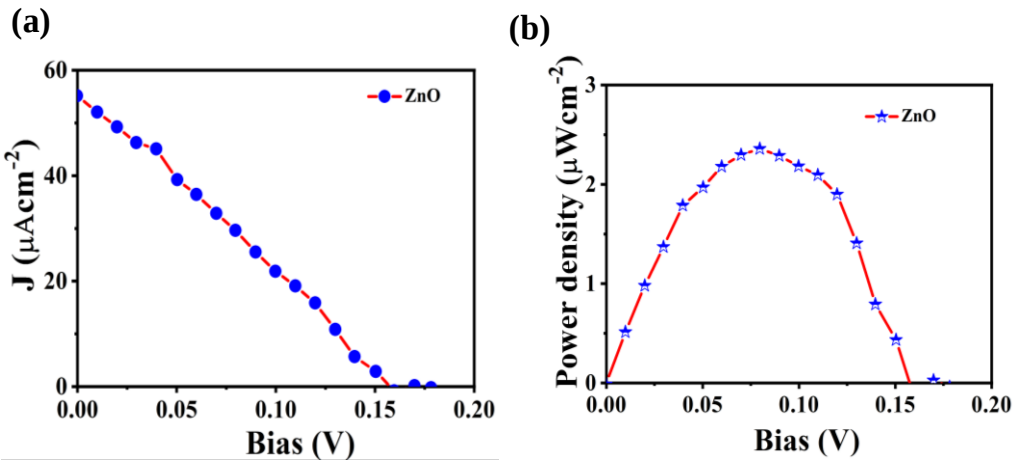

Figure 4. 6: Graph of Current density (a) and power density (b) against voltage

Using the obtained J-V curve and power density curve, various photo voltaic properties such as short circuit current (J_{sc}), Open circuit voltage (V_{oc}), Fill factor (FF) and overall conversion efficiency (η) of the zinc oxide nanoparticles based DSSC were estimated. The Fill factor was calculated using equation 4.7 (Yahia et al., 2016).

$$FF = \frac{J_{\max} V_{\max}}{J_{sc} V_{oc}} \tag{4.7}$$

$$FF = \frac{0.0301 \times 0.0793}{0.000056 \times 161}$$

$$FF = 0.265$$

Where J_{max} and V_{max} are the current density and voltage respectively at maximum power output, J_{sc} is the short circuit current and V_{oc} is an open circuit voltage (Alkuam, 2019). Ruthenium dye N719 was used as photo sensitizer and it was observed that ZnO Nps are very effective in the dye which enhanced the light harvesting. The maximum absorption led to a short circuit current density of 56 μA/cm^2, open circuit voltage of 161 mV, as shown Figure 4.6.

According to the equation 4.7 the calculated FF was 0.265, Based on the obtained FF, the power conversion efficiency of the fabricated DSSC was calculated using the equation 4.8 (Shashanka et al., 2020).

$$\eta = \frac{P\max}{P_{in}} X100\% \qquad (4.8)$$

$$\eta = \frac{0.0301 \times 0.0793}{100} \times 100\ \%$$

$$\eta = 2.4 \times 10^{-2}\ \%$$

Where P_{in} is the incident radiation's power density. The fabricated DSSC demonstrated a light-to- electricity conversion efficiency of $2.4\times10^{--2}$ %, according to equation 4.8.The low PCE of the device may be caused Zn^{2+}/dye clusters that increase the recombination process between the redox(I_3^-) components and the photo injected- electrons (Vittal & Ho, 2017). This greatly limits the number of photo-generated electrons conducted across the external circuit, and thus very low short circuit density. However, its fill factor of 0.297 was remarkably higher than 0.118, reported by Abdullah *et* (Abdullah et al., 2014). These underperformances of ZnO-based photo-anodes are reported in different literature as shown in Table 4.5. This showed that the performance of a cell based on ZnO photo-anode also depends on synthesis techniques that produce NPs with unique properties. The photo

electric performance of the developed DSSC agree with the optical absorption property of the ruthenium dye N719 as observed by other researchers. Table 4.5 shows a comparison between the power conversion efficiency (PCE) obtained in this study and literature values from other researchers.

Table 4. 5: Comparison of PCE for a few selected DSSCs based on ZnO photo-anode

Photo-anode Electrode	**Synthesis method**	**PCE (%)**	**Reference**
ZnO	Hydrothermal	2.9×10^{-1}	(Shaat et al., 2017)
ZnO	solver thermal	2.0×10^{-2}	(Esakki et al., 2021)
ZnO	Chemical bath deposition	3.0×10^{-3}	(Abdullah et al., 2014)
ZnO-2 nm thickness	Screen-printing	8.0×10^{-2}	(Chandiran et al., 2014)
ZnO	Green synthesis	$2.4\ x10^{-2}$	This study

CHAPTER FIVE: CONCLUSION AND RECOMMENDATIONS

5.1 Conclusion

An ecofriendly simple green synthetic method was successfully used to prepare ZnO Nps using *Erythrina abyssinica* stem bark extracts. The NPs of ZnO that were synthesized showed wurtzite hexagonal structure of 65.5 nm average crystallite size at 700 ^{o} C as calculated from Williamson-Hall equation. The study from SEM revealed ZnO Nps in spherical form and are not so much agglomerated. The *Erythrina abyssinica* stem bark extracts acts as both reducing and capping agents there for no extra capping agent was used in this work. An average particle size at 700 ^{o} C of ZnO Nps was found to be 121 nm. The EDX studies revealed the experimental and theoretical 1:1 stoichiometry ratio of zinc and oxygen. Abroad surface absorption peak between 310-377 nm for the annealed ZnO Nps was showed from UV-visible spectroscopy with 3.20, 3.19, 3.16 and 3.12 eV at 300, 400, 500, and 700 ^{o}C respectively as band gaps. Within the green region there were no discernible peaks of E.M (electromagnetic) spectrum, and the photoluminescence spectra of zinc oxide nanoparticles only showed peak in the red and blue portions. A current density- voltage behavior of the manufactured zinc oxide NP based DSSC was investigated using illumination from the solar simulator. With a V_{oc} of 161mV and a 56μA/cm^2 short circuit current density of, the fabricated DSSC demonstrated a PCE of $2.4x10^{-2}$ % . The poor performance of the cell was as result of limited light absorbed in the visible spectrum by the Ru N719 dye adsorbed on biosynthesized ZnO nanoparticles, and fast electron-hole recombination rates.

5.2 Recommendations

The study successfully synthesized ZnO NPs via green synthesis and showed their applicability in DSSCs, thus adding to other areas of application of green-synthesized ZnO NPs such as the biomedical science field, organic electronics, and in environmental applications. Although the study's performance results for DSSC photo-anode application are low compared to other values obtained from chemically synthesized ZnO photo-anodes, the study has paved the way for further research on green-synthesized ZnO NPs for optoelectronic device applications. Future research should be focused on improving the light absorption range of Ru N719 dye adsorbed on biosynthesized ZnO nanoparticles and minimizing the charge recombination rates through doping and heterostructuring.

It is recommended that more research should be done investigations be made by clarifying how various dopants affect zinc oxide photo-anode's band structure and surface modifications. This will provide noticeable benefit in electron transport, increasing DSSC efficiency. Communities should be made aware of the need to preserve this plant species (*Erythrina abyssinicca*) because of its uses in DSSC application.

REFERENCES

Abdullah, H., Omar, A., Razali, M. Z., & Yarmo, M. A. (2014). Photovoltaic properties of ZnO photoanode incorporating with CNTs for dye-sensitized solar cell application. *Ionics*, *20*(7), 1023–1030. https://doi.org/ 10.1007/s11581-013-1038-3

Abebe Abay, A. A. (2018). Nitrogen release dynamics of Erythrina abyssinica and Erythrina brucei litters as influenced by their biochemical composition. *African Journal of Plant Science*, *12(12)*, 331–340.

Aerts, R. (2008). Erythrina abyssinica Lam ex DC. *Plant Resources of Tropical Africa 7(1). Timbers 1*, 249–252. http://database.prota.org/search.htm

Afaq, S., Shah, A. L. I., Sayyad, M. H., Abdulkarim, S., & Qiao, Q. (2018). Step-by-Step Heating of Dye Solution for Efficient Solar Energy Harvesting in Dye-Sensitized Solar Cells. *Journal of Electronic Materials*, *47(8)*(1), 4737–4741. https://doi.org/10.1007/s11664-018-6340-4

Alkuam, E. (2019). An Effective of Dye Molecules with Cadmium Sulfide Nanorods in Dye Sensitized Solar Cell (DSSCs). *Advances in Materials Physics and Chemistry*, *9(04)*(Ii), 37–47. https://doi.org/ 10.4236/ampc.2019.94004

Asahi, A., Hajjaj, F., & Alkoash, A. (2022). Effect of heat and solar radiation on photovoltaic cells. *International Journal of Scientific and Research Publications (IJSRP)*, *12*(5), 144. https://doi.org/ 10.29322/ijsrp. 12.05.2022.p12518

Basnet, P., Inakhunbi Chanu, T., Samanta, D., & Chatterjee, S. (2018). A review

on bio-synthesized zinc oxide nanoparticles using plant extracts as reductants and stabilizing agents. *Journal of Photochemistry and Photobiology B: Biology*, *183*, 201–221. https://doi.org/10.1016/j.jphotobiol.2018.04.036

Bindu, P., & Thomas, S. (2014). Estimation of lattice strain in ZnO nanoparticles: X-ray peak profile analysis. *Journal of Theoretical and Applied Physics*, *8*(4), 123–134. https://doi.org/10.1007/s40094-014-0141-9

Cauda, V., Gazia, R., Porro, S., Stassi, S., Canavese, G., Roppolo, I., & Chiolerio, A. (2014). Nanostructured ZnO Materials: Synthesis, Properties and Applications. *Handbook of Nanomaterials Properties*, *3 (14)*, (pp. 137-177). https://doi.org/10.1007/978-3-642-31107-9

Chandiran, A. K., Abdi-Jalebi, M., Nazeeruddin, M. K., & Grätzel, M. (2014). Analysis of electron transfer properties of ZnO and TiO2 photoanodes for dye-sensitized solar cells. *ACS Nano*, *8*(3), 2261–2268. https://doi.org/ 10.1021/nn405535j

Chandra, I., Singh, S., Senapati, S., Srivastava, P., & Bahadur, L. (2019). Green synthesis of TiO 2 nanoparticles using Bixa orellana seed extract and its application for solar cells. *Solar Energy*, *194*(October), 952–958. https://doi.org/10.1016/j.solener.2019.10.090

Charbonneau, C., Lee, K. E., Shan, G. B., Gomez, M. A., Gauvin, R., & Demopoulos, G. P. (2010). 9(04). *Electrochemical and Solid-State Letters*, *13(8)*, 257–260. https://doi.org/10.1149/1.3429249

Deepa, K. G., Lekha, P., & Sindhu, S. (2012). Efficiency enhancement in DSSC using metal nanoparticles : A size dependent study. *Solar Energy*, *86*(1), 326–330. https://doi.org/10.1016/j.solener.2011.10.007

Esakki, E. S., Sarathi, R., Sundar, S. M., & Devi, L. R. (2021). Materials Today : Proceedings Fabrication of Dye Sensitized Solar Cells using Ixora Macrothyrsa. *Materials Today: Proceedings*, *xxxx*. https://doi.org/10.1016/j.matpr.2021.05.672

Fadhlan, M., Hermandy, S., Zaki, M., Yusoff, M., & Yahya, M. S. (2020). The Green Synthesis of Nanoparticle Zinc Oxide (ZnO) Using Aloe Vera Leaf Extract: Structural and Optical Characterization Reviews. *International Journal of Emerging Trends in Engineering Research*, *8ELECTROLY*(10), 6896–6902. https://doi.org/10.30534/ijeter/2020/448102020

Faisal, S., Jan, H., Shah, S. A., Shah, S., Khan, A., Akbar, M. T., Rizwan, M., Jan, F., Wajidullah, Akhtar, N., Khattak, A., & Syed, S. (2021). Green Synthesis of Zinc Oxide (ZnO) Nanoparticles Using Aqueous Fruit Extracts of Myristica fragrans: Their Characterizations and Biological and Environmental Applications. *ACS Omega*, *6*(14), 9709–9722. https://doi.org/10.1021/acsomega.1c00310

Hong, R. Y., Li, J. H., Chen, L. L., Liu, D. Q., Li, H. Z., Zheng, Y., & Ding, J. (2009). Synthesis, surface modification and photocatalytic property of ZnO nanoparticles. *Powder Technology*, *189*(3), 426–432. https://doi.org/ 10.1016/j .powtec.2008.07.004

Ito, S., Murakami, T. N., Comte, P., Liska, P., Grätzel, C., Nazeeruddin, M. K., & Grätzel, M. (2008). Fabrication of thin film dye sensitized solar cells with solar to electric power conversion efficiency over 10%. *Thin Solid Films*, *516*(14), 4613–4619. https://doi.org/10.1016/j.tsf.2007.05.090

Kishore Kumar, D., Kříž, J., Bennett, N., Chen, B., Upadhayaya, H., Reddy, K. R.,

& Sadhu, V. (2020). Functionalized metal oxide nanoparticles for efficient dye-sensitized solar cells (DSSCs): A review. *Materials Science for Energy Technologies*, *3*, 472-481file:///C:/Users/PERSONAL/Desktop/Research. https://doi.org/10.1016/j.mset.2020.03.003

Kone, W. M., Solange, K. N., & Dosso, M. (2011). Assessing sub-Saharan Erythrina for efficacy: traditional uses, biological activities and phytochemistry. *Pakistan Journal of Biological Sciences: PJBS*, *14*(10), 560–571.

Korir, K., Bii, C., Kiiyukia, C., & Mutai, C. (2011). Antimicrobial activities of Clutia abyssinic and Erythrina abyssinica plants extracts used among the Kipsigis community of Bomet district in Kenya. *Natural Products*, *7*(5), 247–252.

Kumar, S. S., Venkateswarlu, P., Rao, V. R., & Rao, G. N. (2013). Synthesis , characterization and optical propertieses of zinc oxide nanoparticl. *International Nano Letters*, *1 (2013)*, 1–6.

Li, S., Silvers, S. J., & El-Shall, M. S. (1997). Preparation, characterization and optical properties of zinc oxide nanoparticles. *Materials Research Society Symposium - Proceedings*, *452*, 389–394. https://doi.org/10.1557/proc-452-389

Lin, C. H., Chang, S. J., Chen, W. S., & Hsueh, T. J. (2016). Transparent ZnO-nanowire-based device for UV light detection and ethanol gas sensing on c-Si solar cell. *RSC Advances*, *6*(14), 11146–11150. https://doi.org/10.1039/c5ra23028d

Magiswaran, K., Norizan, M. N., Mohamad, I. S., & Mahmed, N. (2021). *Charge*

Recombination in Zinc Oxide-Based Dye-Sensitized Solar Cell : A Mini Review. *14*(December), 14–15.

Mansournia, M., Rafizadeh, S., & Hosseinpour-Mashkani, S. M. (2015). Hydrothermal synthesis, characterization and light harvesting applications of zinc oxide nanostructures. *Journal of Materials Science: Materials in Electronics*, *26*(8), 5839–5846. https://doi.org/10.1007/s10854-015-3144-7

Nuran, A., Zulkifili, B., Kento, T., Daiki, M., & Fujiki, A. (2015). The Basic Research on the Dye-Sensitized Solar Cells (DSSC). *Journal of Clean Energy Technologies 3, 5 (2015)*(5), 382–387. https://doi.org/10.7763/JOCET.2015.V3.228

Pandey, P., Ramzan, M., & Fozia, P. (2016). Effects of annealing temperature optimization on the efficiency of ZnO nanoparticles photoanode based dye sensitized solar cells. *Journal of Materials Science: Materials in Electronics*. https://doi.org/10.1007/s10854-016-5693-9

Rahman, F., Patwary, A. M., Siddique, A. B., Bashar, S., Haque, A., & Akter, B. (2022). Green synthesis of zinc oxide nanoparticles using Cocos nucifera leaf extract : characterization , antimicrobial , antioxidant and photocatalytic activity. *Royal Society Open Science*, *9(11)*, 220858.

Sangeetha, G., Rajeshwari, S., & Venckatesh, R. (2011). Green synthesis of zinc oxide nanoparticles by aloe barbadensis miller leaf extract : Structure and optical properties. *Materials Research Bulletin*, *46*(12), 2560–2566. https://doi.org/10.1016/j.materresbull.2011.07.046

Sha, R., Basak, A., Maity, P. C., & Badhulika, S. (2022). ZnO nano-structured based devices for chemical and optical sensing applications. *Sensors and*

Actuators Reports, *4*, 100098. https://doi.org/10.1016/j.snr.2022.100098

Shaat, S., Zayed, H., Musleh, H., Shurrab, N., Issa, A., Asad, J., & Al Dahoudi, N. (2017). Inexpensive organic dyes-sensitized zinc oxide nanoparticles photoanode for solar cells devices. *Journal of Photonics for Energy*, *7*(2), 025504. https://doi.org/10.1117/1.jpe.7.025504

Shaba, E. Y., Jacob, J. O., Tijani, J. O., & Suleiman, M. A. T. (2021). A critical review of synthesis parameters affecting the properties of zinc oxide nanoparticle and its application in wastewater treatment. In *Applied Water Science* (Vol. 11, Issue 2). Springer International Publishing. https://doi.org/10.1007/s13201-021-01370-z

Sharma, K., Sharma, V., & Sharma, S. S. (2018). Dye-Sensitized Solar Cells: Fundamentals and Current Status. *Nanoscale Research Letters*, *13*. https://doi.org/10.1186/s11671-018-2760-6

Shashanka, R., Esgin, H., Yilmaz, V. M., & Caglar, Y. (2020). nanoparticle based dye-sensitized solar cell. *Journal of Science: Advanced Materials and Devices, 5(2),* pp.185-191. https://doi.org/10.1016/j.jsamd.2020.04.005

Shokry Hassan, H., Kashyout, A. B., Morsi, I., Nasser, A. A. A., & Ali, I. (2014). Synthesis, characterization and fabrication of gas sensor devices using ZnO and ZnO:In nanomaterials. *Beni-Suef University Journal of Basic and Applied Sciences*, *3*(3), 216–221. https://doi.org/https:// doi.org/10.1016/j. bjbas.2014.10.007

Subramanian, N., & Al, A. (2013). A green synthetic route for zinc oxide nanoarchitectures using L -lysine. *Materials Letters*, *92*, 361–364. https://doi.org/10.1016/j.matlet.2012.11.010

Sufyan, M., Mehmood, U., Gill, Y. Q., Nazar, R., Ul, A., & Khan, H. (2021). Hydrothermally synthesize zinc oxide (ZnO) nanorods as an effective photoanode material for third-generation Dye-sensitized solar cells (DSSCs). *Materials Letters*, *297*, 130017. https://doi.org/10.1016/j.matlet.2021.130017

Syed Zahirullah, S., Immanuel, P., Pravinraj, S., Fermi Hilbert Inbaraj, P., & Joseph Prince, J. (2018). Synthesis and characterization of Bi doped ZnO thin films using SILAR method for ethanol sensor. *Materials Letters*, *230*, 1–4. https://doi.org/10.1016/j.matlet.2018.07.067

Tata, S., Chabane, L., Zebbar, N., Trari, M., Kechouane, M., & Rahal, A. (2020). Study of morphological and electrical properties of the ZnO/p-Si hetero-junction: Application to sensing efficiency of low concentration of ethanol vapor at room temperature. *Materials Science in Semiconductor Processing*, *109 (2020)*, 104926. https://doi.org/10.1016/j.mssp.2020.104926

Vittal, R., & Ho, K. (2017). Zinc oxide based dye-sensitized solar cells : A review. *Renewable and Sustainable Energy Reviews*, *70 (2017)*, 920–935. https://doi.org/10.1016/j.rser.2016.11.273

Yahia, I. S., Attieh, S. A., & Hafez, A. A. H. S. (2016). Synthesis and characterization of DSSC by using Pt nano-counter electrode : photosensor applications. *Applied Physics A*, *6 (2016)*, 569. https://doi.org/10.1007/s00339-016-0102-z

Yeh, M., Chang, S., Lin, L., Chou, H., Vittal, R., Hwang, B., & Ho, K. (2015). Size effects of platinum nanoparticles on the electrocatalytic ability of the counter electrode in dye-sensitized solar cells. *Nano Energy*. https://doi.org/

10.1016/j.nanoen.2015.08.008

Zhang, K., Qin, S., Tang, P., Feng, Y., & Li, D. (2020). Ultra-sensitive ethanol gas sensors based on nanosheet-assembled hierarchical ZnO-In2O3 heterostructures. *Journal of Hazardous Materials*, *391*(October 2019), 122191. https://doi.org/10.1016/j.jhazmat.2020.122191

APPENDICES

APPENDIX 1 INTRODUCTORY LETTER

KYAMBOGO UNIVERSITY

P. O. BOX 1 KYAMBOGO
Tel: 041 - 4286792 Fax: 256-41-220464
Website :www.kyu.ac.ug, Email: drgt@kyu.ac.ug

Directorate of Research and Graduate Training

Office of the Director

Date: 11/04/2023

TO WHOM IT MAY CONCERN

RE: BALABYE STEPHEN

Dear Sir/Madam,

This is to introduce to you the above named student Reg: No 21/U/GMSP/14078/PE pursuing MASTER OF SCIENCE IN PHYSICS Department of PHYSICS, Kyambogo University.

She/he intends to carry out research on DYE SENSITIZED SOLAR CELL in partial fulfillment of the requirements for the award of MASTER OF SCIENCE IN PHYSICS

The purpose of this letter therefore is to request you to grant him/her permission to carry out his/her study in your institution.

Any assistance rendered to him/her will be highly appreciated.

Yours sincerely,

for Prof. Bosco Bua
AG. DIRECTOR

KYAMBOGO UNIVERSITY
18 APR 2023
DIRECTOR
DIRECTORATE OF RESEARCH AND GRADUATE TRAINING

LC1 CHAIRPERSON
MATUBA VILLAGE
MAYUGE PARISH
IMANYIRO SUBCOUNTY
MAYUGE DISTRICT
Date: 22/04/2023

Request granted by chairperson Wanamada Moses 075-375-8507

APPENDIX 2: RAW DATA FROM FABRICATED DSSC